Generation of ultrafast magnetic fields from molecular coherent electron currents

Kai-Jun Yuan,[1,2,*] Jing Guo,[1,2,†] and André D. Bandrauk[2,‡]
[1]*Institute of Atomic and Molecular Physics, Jilin University, Changchun, 130012, China*
[2]*Laboratoire de Chimie Théorique, Faculté des Sciences, Université de Sherbrooke, Sherbrooke, Québec, Canada, J1K 2R1*

(Received 23 June 2018; published 5 October 2018)

Coherent electron currents in circular charge transport are of great importance in photoinduced processes, magneto-optics, and reaction dynamics of molecules. We present ultrafast magnetic field generation by circularly polarized attosecond ultraviolet laser pulses in molecular media. Simulations in a one electron molecular model H_2^+ show that the induced magnetic field exhibits periodic oscillations on attosecond time scales, which depends on the laser pulse and molecular alignment. We attribute it to the coherent electronic currents, arising from resonant coherent excitation between the ground and excited electronic states. The temporal evolution of the generated magnetic fields and the induced electronic currents relies on the molecular orbital superposition in the electron coherence, providing a way for controlling ultrafast magnetic field generation.

DOI: 10.1103/PhysRevA.98.043410

I. INTRODUCTION

Rapid developments of ultrafast laser technology allow one to study electronic dynamics on its natural time scale, the attosecond (1 as $= 10^{-18}$ s) [1,2]. High order harmonic generation (HHG) by linear polarization ionization recombination is the main source of isolated attosecond pulses [3,4]. Currently, 43 as pulses are the shortest available pulses for new ultrafast optical imaging [5]. Alternatively, optically induced magnetic fields have also been adopted as a tool for investigations of new phenomena in molecular and material sciences, including molecular paramagnetic bonding [6], nonequilibrium electronic processes [7], demagnetization processes [8], coherent ultrafast magnetism [9], and optical magnetic recording [10]. These magnetization phenomena are currently studied with femtosecond circular-polarization x-ray sources due to their nanometer resolution and ultrarapid response shorter than physical relaxation times [11–14]. It has been found that one can efficiently produce magnetic fields in molecules from electronic ring currents. By quantum-chemical numerical simulations unidirectional constant valence-type electronic currents and associated static magnetic fields [15,16] can be generated by means of circularly polarized π attosecond UV laser pulses resonant with degenerate π orbitals. Results show that the laser-induced magnetic fields from electronic currents are static and can be much larger than those obtained by traditional static field methods [17]. Moreover, linearly polarized laser pulses can also be used to induce ring currents in degenerate excited states by controlling the rotation direction of π electrons in planar or nonplanar aromatic molecules [18]. The driving laser pulses can be optimized as well by optimal control theory [19]. In general, single electron states or the continuum are used to produce electron currents and static magnetic fields [15,16] or time-dependent fields [20,21].

In this work we present a scheme to produce ultrafast magnetic fields by intense attosecond circularly polarized UV pulses in molecules. We consider the process from a coherent electronic superposition state, created by a resonant excitation. Recently, investigations of ultrafast electronic dynamics in an initial coherent state have been attracting considerable attention [22–24]. It has been shown that an intense ultrafast pump pulse can induce electron charge transport across a molecular structure [25–30] by the coherent excitation of electronic states. The pure electron response offers a possibility for quantum control of molecular reactions on the attosecond time scale. By preparing a coherent electronic state with a laser pulse, electron currents can also be produced in ring molecules which has been adopted as a source of ultrafast magnetic field generation [16,20]. It is found that electron coherences and electron currents inside molecular benzene are functions of the polarization and helicity of the laser pulse, and the symmetry property of the excited electronic state [29]. Advanced high harmonic spectroscopy and photoelectron momentum spectra have been used to directly measure and control electron coherence and charge migration dynamics [30–32]. We focus on ultrafast magnetic field generation from coherent electron currents. Simulations are performed on aligned H_2^+ from numerical solutions of time-dependent Schrödinger equations (TDSEs). We adopt a wavelength $\lambda = 70$ nm circularly polarized laser pulse, resonant with the $1s\sigma_g - 2p\pi_u$ states. Because of the multiple state excitation by circularly polarized pulses, coherent superposition of electronic states gives rise to coherent electron currents inside molecules, thus leading to the generation of attosecond magnetic fields. It is found that the resulting strong magnetic fields oscillate periodically, arising from coherent combinations of electronic circular wave packets. Strongest magnetic fields are generated both in time and space on and around nuclei due to electron current localization in molecular planes.

*kaijun.yuan@usherbrooke.ca
†gjing@jlu.edu.cn
‡andre.bandrauk@usherbrooke.ca

The paper is arranged as follows: In Sec. II, we briefly describe the computation methods. The numerical results by solving TDSEs for aligned H_2^+ are presented and discussed in Sec. III. Finally, we summarize our findings in Sec. IV. Throughout this paper, atomic units (a.u.) are used unless otherwise noted.

II. NUMERICAL METHODS

Within a static [Born-Oppenheimer approximation BOA] nuclear frame, molecular TDSEs read as

$$i\nabla_t\psi(\mathbf{r},t) = [\hat{H}_0(\mathbf{r}) + \mathbf{r}\cdot\mathbf{E}(t)]\psi(\mathbf{r},t). \quad (1)$$

$H_0(\mathbf{r}) = T(\mathbf{r}) + V_c(\mathbf{r})$ is the field free molecular Hamiltonian. The corresponding three-dimensional (3D) TDSE is solved using cylindrical coordinates $\mathbf{r} = (\rho,\theta,z)$ with the plane $x = \rho\cos\theta$ and $y = \rho\sin\theta$, as illustrated in Fig. 1. The molecular kinetic energy term can be written as

$$T(\rho,\theta,z) = -\frac{1}{2}\left[\frac{1}{\rho}\frac{\partial}{\partial\rho}\rho\frac{\partial}{\partial\rho} + \frac{1}{\rho^2}\frac{\partial^2}{\partial^2\theta} + \frac{\partial^2}{\partial^2 z}\right]. \quad (2)$$

$V_c(\mathbf{r})$ is the molecular Coulomb potential where a soft parameter is used to remove the singularity and accurate production of the electronic state potential energies of H_2^+ [33]. For H_2^+ at equilibrium $R_e = 2$ a.u., the eigenenergies of the three lowest electronic states, the ground $1s\sigma_g$ state, the first excited $2p\sigma_u$ state, and the second degenerate excited $2p\pi_u$ state, are, respectively, $E_{\sigma_g} = -0.58$ a.u., $E_{\sigma_u} = -0.15$ a.u., and $E_{\pi_u} = 0.07$ a.u. The corresponding ground-state dissociation energy $E_d = E_\infty - E_{\sigma_g} = 0.08$ a.u. The molecular ion is prealigned before ionization and this can be readily achieved with current laser technology [34]. The radiative interaction between the laser field and the electron is described by $\mathbf{r}\cdot\mathbf{E}(t) = \hat{e}_x\rho\cos\theta E_x(t) + \hat{e}_y\rho\sin\theta E_y(t)$ in the length gauge for circularly polarized laser pulses,

$$\mathbf{E}(t) = E_0 f(t)[\hat{e}_x\cos(\omega t) + \hat{e}_y\sin(\omega t)], \quad (3)$$

propagating in the z direction and $\hat{e}_{x/y}$ is the field polarization direction. The laser polarization corresponds to positive (right) helicity. A smooth $\sin^2(\pi t/n\tau)$ pulse envelope $f(t)$ for maximum amplitude E_0 and intensity $I_0 = \frac{1}{2}c\varepsilon_0 E_0^2$ is adopted, where one optical cycle $\tau = 2\pi/\omega$. This pulse

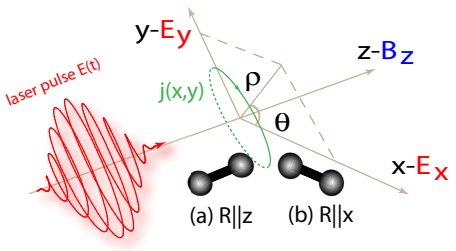

FIG. 1. Illustration of ultrafast magnetic field generation by a circularly polarized UV laser pulse with its field vector polarized in the ($x = \rho\cos\theta$, $y = \rho\sin\theta$) plane, propagating along the z axis. $j(x,y)$ denotes induced electron currents in the laser polarization plane and B_z presents the generated magnetic field along the z axis. Two cases for different molecular alignments (a) $R||z$ and (b) $R||x$ are compared.

satisfies the total zero area $\int E(t)dt = 0$. The 3D TDSE is solved numerically by a second order split operator method in the time step δt combined with a fifth order finite difference method and Fourier transform technique in the spatial steps $\delta\rho$, δz, and $\delta\theta$ [35,36]. The time step is taken to be $\delta t = 0.01$ a.u.=0.24 as. The spatial discretization is $\delta\rho = \delta z = 0.25$ a.u. for a radial grid range $0 \leqslant \rho \leqslant 128$ a.u. (6.77 nm) and $|z| \leqslant 32$ a.u. (1.69 nm), and the angle grid size $\delta\theta = 0.025$ radian. To prevent unphysical effects due to the reflection of the wave packet from the boundary, we multiply $\psi(\rho,\theta,z,t)$ by a "mask function" or absorber in the radial coordinates ρ with the form $\cos^{1/8}[\pi(\rho-\rho_a)/2\rho_{abs}]$. For all results reported here we set the absorber domain $\rho_a = \rho_{max} - \rho_{abs} = 104$ a.u. with $\rho_{abs} = 24$ a.u., exceeding well the field induced electron excursion $\alpha_d = E_0/\omega^2$ of the electron.

The time-dependent electron current density in the molecular ionization process is defined by the quantum expression,

$$\mathbf{j}(\mathbf{r},t) = \frac{i}{2}[\psi(\mathbf{r},t)\nabla_\mathbf{r}\psi^*(\mathbf{r},t) - \psi^*(\mathbf{r},t)\nabla_\mathbf{r}\psi(\mathbf{r},t)], \quad (4)$$

where $\psi(\mathbf{r},t)$ is the exact BOA electron wave function obtained from Eq. (1) and $\nabla_\mathbf{r} = \mathbf{e}_\rho\nabla_\rho + \mathbf{e}_\theta\frac{1}{\rho}\nabla_\theta + \mathbf{e}_z\nabla_z$ in cylindrical coordinates. Then the corresponding induced time-dependent magnetic fields are calculated using the following classical Jefimenko's equation [37],

$$\mathbf{B}(\mathbf{r},t) = \frac{\mu_0}{4\pi}\int\left[\frac{\mathbf{j}(\mathbf{r}',t_r)}{|\mathbf{r}-\mathbf{r}'|^3} + \frac{1}{|\mathbf{r}-\mathbf{r}'|^2 c}\frac{\partial\mathbf{j}(\mathbf{r}',t')}{\partial t}\right] \times(\mathbf{r}-\mathbf{r}')d^3\mathbf{r}', \quad (5)$$

where $t_r = t - r/c$ is the retarded time and $\mu_0 = 4\pi\times 10^{-7}$ NA^{-2} (6.692×10^{-4} a.u.). For the static time-independent conditions occurring after the laser pulse, then Eq. (5) reduces to the classical Biot-Savart law [37] $\mathbf{B}(\mathbf{r},t) = \frac{\mu_0}{4\pi}\int\frac{\mathbf{j}(\mathbf{r}',t)\times(\mathbf{r}-\mathbf{r}')}{|\mathbf{r}-\mathbf{r}'|^3}d^3\mathbf{r}'$.

III. RESULTS AND DISCUSSIONS

We first consider the case of ultrafast magnetic field generation in the molecule H_2^+ at equilibrium aligned along the z axis, $R||z$ in Fig. 1, perpendicular to the laser (x,y) polarization plane. Since the induced electron currents by the circularly polarized pulse are localized in the laser (x,y) plane, the generated magnetic field mainly lies along the z axis, as illustrated in Fig. 1. We therefore only present the results $B_z(\mathbf{r},t)$. Figure 2 displays the generated magnetic field $B_z(\mathbf{r}=0,t)$ at the molecular center by circularly polarized attosecond laser pulses. The molecular initial wave function is prepared in the ground $1s\sigma_g$ state calculated by propagating an appropriate test wave function in imaginary time using the zero-field TDSE in Eq. (1). The pulse intensity $I_0 = 3.5\times10^{14}$ W/cm^2 ($E_0 = 0.1$ a.u.) and duration 5τ (optical cycles, o.c.), corresponding to 580 as full width at half maximum (FWHM) are used. We choose the pulse wavelength $\lambda = 70$ nm ($\omega = 0.65$ a.u.), resonant with the $\sigma_g - \pi_u$ excitation in H_2^+ at equilibrium $R_e = 2$ a.u.. For comparison, results of $B_z(\mathbf{r}=0,t)$ by $\lambda = 30$ nm ($\omega = 1.52$ a.u.) and $\lambda = 100$ nm (0.456 a.u.) circularly polarized pulses are also presented in Fig. 2. Such pulses create currents with a maximum radius

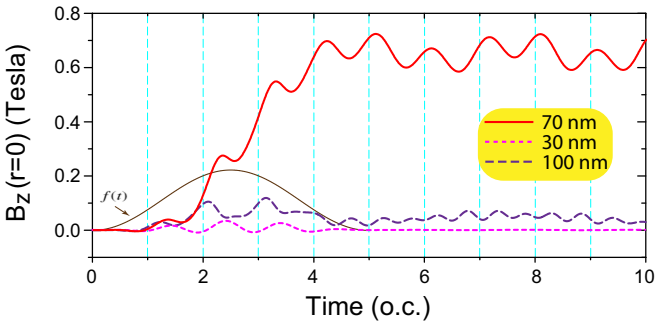

FIG. 2. Generation of ultrafast magnetic fields $B_z(\mathbf{r}=0,t)$ in the molecule H_2^+ aligned along the z axis, perpendicular to the laser (x, y) polarization plane, Fig. 1(a), by attosecond circularly polarized UV laser pulses at (solid line) $\lambda = 70$ nm ($\omega = 0.65$ a.u.), (dotted line) 30 nm (1.52 a.u.), and (dashed line) 100 nm (0.456 a.u.). The pulse intensity $I_0 = 3.5 \times 10^{14}$ W/cm^2, and durations 5τ, where $\tau = 2\pi/\omega$, (i.e., 1 o.c. is 232 as for 70 nm, 99 as for 30 nm, and 331 as for 100 nm) are fixed. Gray thin line denotes the pulse envelope $f(t)$.

around the z axis, $r_c \leqslant 2E_0/\omega = 1.0$ a.u. (at $\lambda = 100$ nm) [20].

In Fig. 2 we see that time-dependent magnetic fields oscillate following the circularly polarized pulses. The induced magnetic fields $\mathbf{B}_z(r=0,t)$ are, however, shown to be sensitive to the pulse wavelength. At $\lambda = 70$ nm, strong magnetic fields with the maximum value $B_z = 0.72$ T [(Tesla) 1 T = 10^4 Gauss] at the molecular center are obtained, whereas for the cases at $\lambda = 30$ nm and 100 nm, the maximum induced magnetic fields are, respectively, weak $B_z = 0.04$ T and 0.1 T due to nonresonance and the radius of electron currents $\sim E_0/\omega^2$ [20], as discussed below. The enhancements of the induced magnetic fields at $\lambda = 70$ nm mainly result from the resonant excitation between the $1s\sigma_g$ and $2p\pi_u$ electronic states. Of note is that after the pulses switch off (>5 o.c.), strong magnetic fields remain. The oscillations with a period $\Delta\tau = \tau = 2\pi/\omega$, the same as the pulse, illustrate the electron coherence of the currents in the molecule.

The circularly polarized pulse at $\lambda = 70$ nm [$\omega = 0.65$ a.u.$= I_p(2p\pi_u^+) - I_p(1s\sigma_g) = 0.65$ a.u.], where I_p are the molecular ionization potentials, leads to a $\sigma_g - \pi_u^+$ ($\Delta m = +1$) resonant excitation. As a result, a coherent superposition state of the two electronic states, the $1s\sigma_g$ state and the $2p\pi_u^+$ state of positive (right) helicity, is created. The wave function of the coherent superposition state is expressed as

$$\psi_0^{(1)}(\mathbf{r},t) = c_{\sigma_g}\psi_{\sigma_g}(\mathbf{r})e^{-iE_{\sigma_g}t} + c_{\pi_u^+}\psi_{\pi_u^+}(\mathbf{r})e^{-iE_{\pi_u^+}t}. \quad (6)$$

$\psi_{\sigma_g/\pi_u^+}(\mathbf{r})$ and E_{σ_g/π_u^+} are the wave functions and energies of the ground or excited state, and c_{σ_g} and $c_{\pi_u^+}$ are the occupation coefficients. The corresponding time-dependent coherent electron density distributions are described by

$$\begin{aligned}\mathcal{A}(\mathbf{r},t) &= \left|\psi_0^{(1)}(\mathbf{r},t)\right|^2 \\ &= \mathcal{A}^{(\sigma_g)}(\mathbf{r}) + \mathcal{A}^{(\pi_u^+)}(\mathbf{r}) + \mathcal{A}^{(\sigma_g,\pi_u^+)}(\mathbf{r},t). \quad (7)\end{aligned}$$

The coherent electron dynamics is composed of the two electronic state densities, $\mathcal{A}^{(\sigma_g)}(\mathbf{r}) = |c_{\sigma_g}\psi_{\sigma_g}(\mathbf{r})|^2$ and $\mathcal{A}^{(\pi_u^+)}(\mathbf{r}) = |c_{\pi_u^+}\psi_{\pi_u^+}(\mathbf{r})|^2$ state, and their interfering superposition,

$$\mathcal{A}^{(\sigma_g,\pi_u^+)}(\mathbf{r},t) = c_{\sigma_g}c_{\pi_u^+}\psi_{\sigma_g}(\mathbf{r})\psi_{\pi_u^+}(\mathbf{r})e^{-i\Delta Et} + \text{c.c.}, \quad (8)$$

where $\Delta E = E_{\pi_u^+} - E_{\sigma_g}$ is the energy difference between the two $1s\sigma_g$ and $2p\pi_u^+$ electronic states. $\mathcal{A}^{(\sigma_g)}(\mathbf{r})$ and $\mathcal{A}^{(\pi_u^+)}(\mathbf{r})$ are time independent. The superposition term $\mathcal{A}^{(\sigma_g,\pi_u^+)}(\mathbf{r},t)$ as a function of time t describes the attosecond coherent electronic charge migration [30] with the oscillation period $\Delta\tau^{(0)} = 2\pi/\Delta E = 232$ as $= \tau$. During the pulse excitation, the population in the excited state increases gradually. The $\sigma_g - \pi_u^+$ resonant excitation with angular momentum $\Delta m = +1$ for positive (right) helicity leads to circular electron currents around the molecular axis. As a result, strong magnetic fields are induced. The increase of the magnetic field $B_z(t)$ with time in Fig. 2 results from the increase of the population and currents. After the pulse $t > 5\tau$, state occupation coefficients are constant, where $|c_{\sigma_g}(t)|^2 = |\langle\psi_{\sigma_g}(\mathbf{r})|\psi(\mathbf{r},t)\rangle|^2 = 0.2$ and $|c_{\pi_u^+}(t)|^2 = |\langle\psi_{\pi_u^+}(\mathbf{r})|\psi(\mathbf{r},t)\rangle|^2 = 0.4$. Combining Eqs. (4)–(8) we see that the evolution of the magnetic fields with time arises from the coherent superposition of the two electronic states.

For the excited $2p\pi_u^+$ electronic state in Fig. 1(a), the wave function can be written as $\psi_{\pi_u^+}(\mathbf{r}) = [\psi_{\pi_u}^x + i\psi_{\pi_u}^y]/\sqrt{2} = \widetilde{\psi}_{\pi_u}e^{-i\eta}$, $|\widetilde{\psi}_{\pi_u}|^2 = [|\psi_{\pi_u}^x|^2 + |\psi_{\pi_u}^y|^2]/2$, and $\psi_{\pi_u}^x$ and $\psi_{\pi_u}^y$ are the degenerate real orbital components [38]. The phase η is defined as $\eta = \tan^{-1}[|\psi_{\pi_u}^y|/|\psi_{\pi_u}^x|]$. The induced electron currents in molecules can be described by the electronic angular continuity equation [28,29],

$$\frac{d}{dt}\mathcal{A}^+(t) + \frac{\partial}{\partial\theta}j_\theta^+(t) = 0. \quad (9)$$

For the perpendicular polarization case of $R||z$, Fig. 1(a), the interfering term in Eq. (8) can be expressed as

$$\mathcal{A}^+(t) \sim 2\left|c_{\sigma_g}(t)c_{\pi_u^+}(t)\right|\psi_{\sigma_g}\widetilde{\psi}_{\pi_u}\cos(\Delta Et - \theta), \quad (10)$$

since $\theta = \eta$. Consequently, the time-dependent electronic density $\mathcal{A}(t)$ and angular currents $j_\theta(t)$ evolve around the molecular axis with the same period of $\tau = 2\pi/\Delta E$. The induced magnetic field is therefore a function of time t, i.e, $B_z(t) \sim \cos(\Delta Et)$.

For the case of a $\lambda = 30$ nm ($\omega = 1.52$ a.u.) circularly polarized laser pulse, a direct single photon ionization process dominates since $\omega > I_p$ ($I_p = 1.1$ a.u.). Magnetic fields mainly come from the free electron in the continuum. As shown in Eq. (4), the laser-induced electron current j is a product of the continuum electron density (ionization probability) $\mathcal{A}(\mathbf{r},t) = |\psi(\mathbf{r},t)|^2$, and the laser-induced velocity v (or $\nabla\mathbf{r}$), i.e., $j \sim \mathcal{A}v$. From Eq. (5) one obtains that the generated magnetic field $B_z(\mathbf{r}=0,t)$ at the molecular center is shown to be directly proportional to the induced electron current j and inversely proportional to the current radius r, which then can be simplified to $B_z \sim \mathcal{A}v/r$. The magnetic field then can be decomposed into two components, the ionized electron density $\mathcal{A}$ and a ratio of the electron velocity and radius, $\kappa = v/r$. $\mathcal{A}$ corresponds to the transition amplitudes, which are determined by the intrinsic transition dipole of molecules and the electric field strength. The ratio κ is determined by the pulse amplitude and frequencies. At wavelength $\lambda = 30$ nm, the electron is released from the molecular medium quickly

with a large radius since $r \sim 1/\omega^2$ [20]. As a result, weak magnetic fields are induced. After the pulse switches off, the quick spread of the electronic wave packets in the continuum suppresses the induced magnetic field generation.

It is found that at $\lambda = 100$ nm, the direct transition between the ground $1s\sigma_g$ state and the excited $2p\sigma_u$ state is forbidden due to select rules for circular polarization. However, such ultrashort circularly polarized laser pulse can induce coherent Rydberg circular electronic wave packets with the δ_g orbital symmetry by absorbing two photons since $2\omega \lesssim I_p$. The corresponding wave function of the coherent electronic state is

$$\psi_0^{(2)}(\mathbf{r}, t) = c_{\sigma_g}\psi_{\sigma_g}(\mathbf{r})e^{-iE_{\sigma_g}t} + c_{\mathrm{Ryd}}\psi_{\mathrm{Ryd}}(\mathbf{r})e^{-iE_{\mathrm{Ryd}}t}, \quad (11)$$

where ψ_{Ryd}, c_{Ryd}, and E_{Ryd} are the wave function, occupation coefficient, and energy of Rydberg states. The corresponding energy difference between the coherent states is $\Delta E = 2\omega = 0.912$ a.u.. As shown in Fig. 2, the oscillations of the induced magnetic field are composed of two stages: At the first stage ($t < 5$ o.c.) the induced magnetic field follows the laser pulse with period $\tau = 2\pi/\omega$ and after the pulse ($t > 5$ o.c.), it oscillates with a period $\Delta\tau = \tau/2$, confirming the coherent Rydberg wave packets. For the two photon $\lambda = 100$ nm case, the excitation probability is smaller than that of the single photon $\lambda = 70$ process. Consequently, weak magnetic fields with the maximum value $B_z = 0.1$ T are induced in Fig. 2. In Rydberg states the coherent circular wave packets also spread spatially. As a result the evolution of the induced magnetic field with time decreases gradually in amplitude.

The generated magnetic fields have also been shown to be sensitive to the geometry of the molecular orbitals. We next present magnetic field generation at different molecular alignments. Figure 3 shows results of induced magnetic fields at the nuclear centers $\mathbf{r} = \pm\mathbf{R}/2$ and the molecular center $\mathbf{r} = 0$ by the $\lambda = 70$ nm circularly polarized laser pulse. The other parameters are the same as in Fig. 2. Two cases of molecular alignments, (a) $R||z$ where $(e_x, e_y) \perp \mathbf{R}$ and (b) $R||x$ with $e_x \parallel R$, as illustrated in Fig. 1, are compared. It is found that periodical oscillations of magnetic fields are generated for both alignments. For the case of the molecular internuclear axis perpendicular to the laser polarization plane, $R||z$, the same magnetic fields are produced at two nuclei, $B_z(\mathbf{r} = -\mathbf{R}/2, t) = B_z(\mathbf{r} = +\mathbf{R}/2, t)$ with the maximum value 0.61 T. The magnetic field at the molecular center $B_z(\mathbf{r} = 0, t)$ is slightly larger than those at the nuclei $\pm\mathbf{R}/2$. However, for the case of the molecule parallel to the laser polarization plane, $R||x$, the induced magnetic field $B_z(\mathbf{r}, t)$ is strongly dependent on the measurement position $\mathbf{r}$. The time-dependent magnetic fields at the nuclei $\mathbf{r} = \pm\mathbf{R}/2$ oscillate periodically with opposite phases, $B_z(\mathbf{r} = -\mathbf{R}/2, t) \approx -B_z(\mathbf{r} = +\mathbf{R}/2, t)$ with maximum field strength 0.83 T. At the molecular center the induced magnetic field $B_z(\mathbf{R} = 0, t)$ is suppressed where the maximum field is 0.3 T. The dependence of induced magnetic fields on the molecular alignment indicates the different orbital combinations and evolutions of the coherent electronic wave packets.

For the case of the molecular axis parallel to the laser polarization plane, $R||x$, the resonant $\sigma_g - \pi_u$ excitation corresponds to a perpendicular transition. The coherent excited

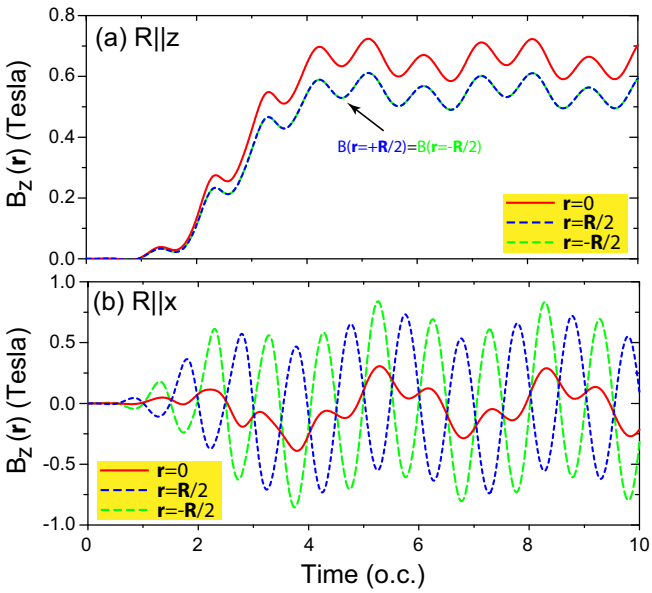

FIG. 3. Evolutions of the induced magnetic field $B_z(\mathbf{r}, t)$ at the molecular center $\mathbf{r} = 0$ and the nuclei $\mathbf{r} = \pm\mathbf{R}/2$ in H_2^+ aligned along (a) the z and (b) x axes by $\lambda = 70$ nm ($\omega = 0.65$ a.u.) attosecond circularly polarized UV laser pulses, as illustrated in Fig. 1. The pulse intensity $I_0 = 3.5 \times 10^{14}$ W/cm^2 ($E_0 = 0.1$ a.u.) and duration 5τ, (o.c.), corresponding to 580 as FWHM are used.

state is then given by [39]

$$\psi_{\pi_u}(\mathbf{r}) = -i\left[\psi_{\pi_u^+}(\mathbf{r}) - \psi_{\pi_u^-}(\mathbf{r})\right]/\sqrt{2} = \psi^y_{\pi_u}, \quad (12)$$

where $\psi_{\pi_u^\pm} = \psi^z_{\pi_u} \pm i\psi^y_{\pi_u}$. The corresponding time-dependent electron density distribution of the interference term is

$$\mathcal{A}(t) \sim -\left|c_{\sigma_g}c_{\pi_u^\pm}\right|\psi_{\sigma_g}\tilde{\psi}_{\pi_u^\pm}\cos(\Delta E t)\sin(\eta). \quad (13)$$

Combination of Eqs. (9) and (13) shows that the electron density distributions and the angular electron currents evolve periodically with a period $2\pi/\Delta E$, leading to a periodical oscillation of the induced magnetic field $B_z(\mathbf{r}, t)$ in Fig. 3(b). Of note is that the coherent electron wave packets and corresponding angular electron currents move mainly along the y axis, perpendicular to the molecular axis due to $\mathcal{A}(t) \sim \sin(\Delta E t)\cos(\eta)$ since the $\sigma_g - \pi_u$ transition is an allowed perpendicular transition induced by E_y [Fig. 1(b)].

We show in Fig. 4 induced spatiotemporal electron currents at various moments after the $\lambda = 70$ nm circularly polarized pulse duration. Results are calculated numerically by $j_\theta(x, y, z = 0, t) = j_\theta(\rho, \theta, z = 0, t)$ in Eq. (4). Varying the time t leads to a period evolution of 232 as, the same as in Fig. 2 for the magnetic field. As predicted in Eqs. (10) and (13), the electron current $j_\theta(x, y, t)$ is determined by the function $\cos(\Delta E t)$, giving rise to the periodical evolution of $2\pi/\Delta E = \tau$, as shown in Fig. 4. The maximum and minimum of electron currents $j_\theta(t)$ are mirror images of each other at time $t \to t + \tau/2$, confirming the period of the electron coherence.

In Fig. 4(a) for the perpendicular field polarization case, $R||z$, the induced electron currents evolve with an anticlockwise direction around the molecular axis, generating unidirectional magnetic fields along the molecular axis [Fig. 3(a)]. As

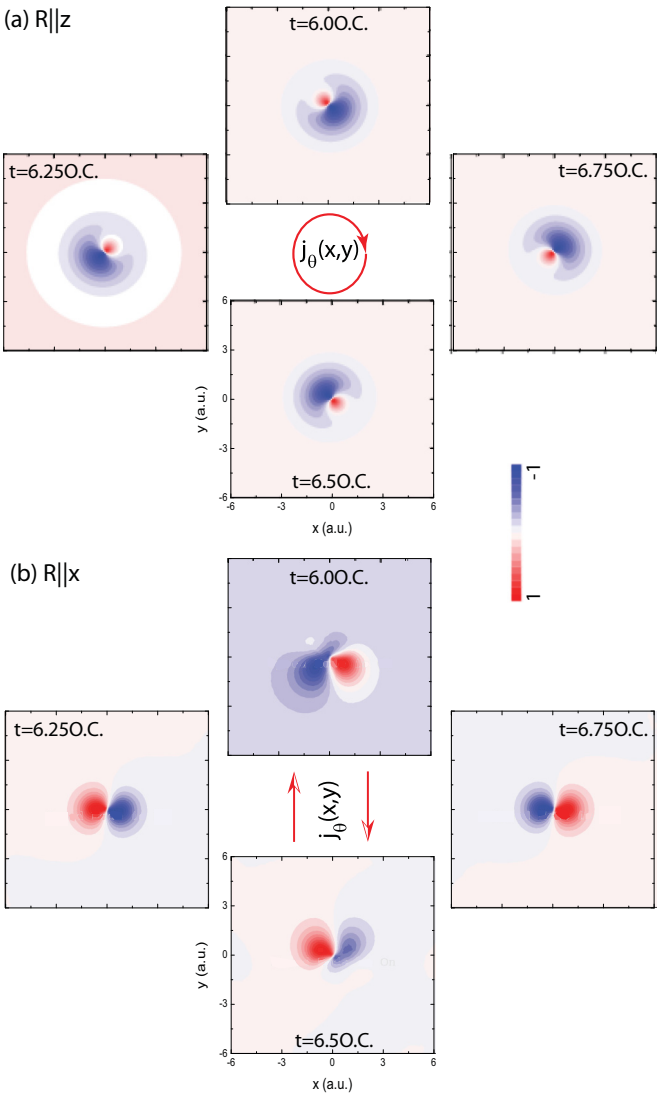

FIG. 4. Contour density plots of induced angular electron currents $j_\theta(x, y, t)$ at $z = 0$ at different moments of the molecular ion H_2^+ at equilibrium $R_e = 2$ a.u. after the $\lambda = 70$ nm and 5 o.c. circularly polarized pulse $\mathbf{E}(t)$ with its field vector polarized in the (x, y) plane. Two cases of the molecule aligned along the (a) z and (b) x axes, i.e., perpendicular and parallel to the laser polarization plane; c.f. Fig. 3. Arbitrary units of distributions are used.

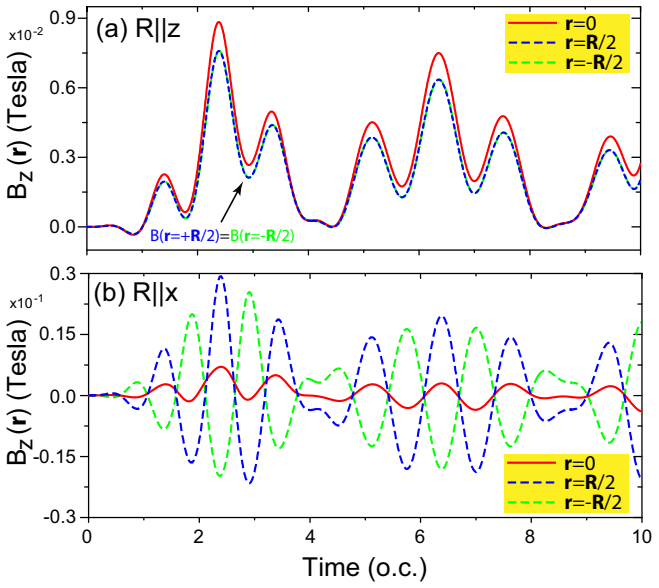

FIG. 5. Time-dependent magnetic field generation $B_z(\mathbf{r}, t)$ at the molecular center $\mathbf{r} = 0$ and the nuclei $\mathbf{r} = \pm\mathbf{R}/2$ in H_2^+ aligned along (a) the z axis and (b) the x axis by $\lambda = 50$ nm ($\omega = 0.91$ a.u.) attosecond circularly polarized UV laser pulses, as illustrated in Fig. 1. The pulse intensity $I_0 = 3.5 \times 10^{14}$ W/cm^2 ($E_0 = 0.1$ a.u.) and duration 5τ, (1 o.c.=165.6 as) are used.

a consequence of the equivalent electronic densities on the two nuclei $\pm R/2$, i.e., $|\psi(-R/2, t)|^2 = |\psi(+R/2, t)|^2$, the similar magnetic fields are produced in Fig. 3(a), $B_z(-R/2, t) = B_z(+R/2, t)$. At the molecular center $\mathbf{r} = \mathbf{0}$, the electron wave function is the overlap between the two nuclear orbitals. Therefore, the generated magnetic fields are the sum of those at the nuclei $\pm R/2$, i.e., $B_z(0, t) \sim B_z(-R/2, t) + B_z(+R/2, t)$. Their overlap enhances the magnetic fields at the molecular center. However, for the parallel field-molecule case, $R||x$, in Fig. 4(b), the induced electron currents oscillate periodically in the up ($y > 0$) and down ($y < 0$) direction, perpendicular to the molecular R or x axis. As a result, the generated magnetic fields on the nuclei vary periodically and show opposite phases. As shown in Fig. 4(b), when the electron current goes up, the magnetic field on the right nuclear center is positive whereas that on the left is negative. Altering the electron currents leads to a reverse process. Their superposition with opposite phases gives rise to suppression of generated magnetic fields at the molecular center $B_z(\mathbf{r} = \mathbf{0}, t)$. Due to the helicity effect of the circularly polarized laser pulse, the strengths of the generated magnetic fields on the two nuclei are not equal at the same time, $|B_z(-R/2, t)| \neq |B_z(+R/2, t)|$. Consequently, the time-dependent magnetic field $B_z(0, t)$ at the molecular center has been induced in Fig. 3(b).

The angular spread of the molecular alignment may decrease the coherent excitation and charge migration, leading to a suppression of magnetic field generation. As shown in Figs. 2–4 the generated magnetic field $B_z(\mathbf{r}, t)$ depends on the measurement position $\mathbf{r}$ and the symmetry of the coherent superposition state, i.e., the molecular alignments. Therefore, the angular spread does not influence significantly the magnetic field generation. Moreover, the circularly polarized laser pulse has equal field amplitudes in each orthogonal direction which decrease such suppression of the generated magnetic field.

We finally present the process of generating time-dependent magnetic fields $B_z(\mathbf{r}, t)$ in the aligned molecular ion H_2^+ by a Rydberg resonant $\lambda = 50$ nm ($\omega = 0.911$ a.u.) and 5τ circularly polarized laser pulse. Figure 5 displays the results of magnetic fields $B_z(\mathbf{r}, t)$ with different molecular alignments (a) $R \parallel z$ and (b) $R \parallel x$. The other laser parameters are the same as in Fig. 3. We also measure the magnetic field $B_z(\mathbf{r}, t)$ at the three positions, the two nuclei $\mathbf{r} = \pm\mathbf{R}/2$ and the molecular center $\mathbf{r} = 0$ as a function of time t. Similar phenomena are obtained in Fig. 5, as the processes by the $\sigma_g - \pi_u$ resonant $\lambda = 70$ nm

pulse in Fig. 3. Oscillations of the time-dependent generated magnetic fields are produced again with period $\tau = 2\pi/\omega = 165.6$ as. For the perpendicular field-molecule case, $R \parallel z$, the induced magnetic fields at the two nuclei are the same $B_z(\mathbf{r} = -\mathbf{R}/2, t) = B_z(\mathbf{r} = \mathbf{R}/2, t)$ whereas for the parallel case, $R \parallel x$, the magnetic fields $B_z(\mathbf{r} = -\mathbf{R}/2, t) \approx -B_z(\mathbf{r} = \mathbf{R}/2, t)$ with opposite phases. This process corresponds to a coherent superposition between the ground $1s\sigma_g$ state and excited Rydberg states, as predicted in Eq. (10). The $\lambda = 50$ nm circularly polarized laser pulse creates coherent Rydberg circular polarization electronic wave packets with π_u orbital symmetries after one ω photon absorption. As illustrated in Fig. 4, the different molecular alignments therefore lead to distinct evolution processes of induced electron currents and generated magnetic fields by circularly polarized pulses.

IV. CONCLUSIONS

Ultrafast magnetic fields generated from molecular coherent electron currents by circularly polarized attosecond laser pulses have been studied by numerically solving TDSEs. The single electron molecular ion H_2^+ as a benchmark system is used to illustrate the effects of the electron current coherence. It is found that a circularly polarized pulse creates a coherent superposition of ground and excited electronic states and attosecond time-dependent electronic ring currents inside molecules, leading to oscillating magnetic field pulse generation in real time. Such ultrafast intramolecular electronic currents are controlled by the symmetry of the molecular orbitals. The orbital properties of molecules are essential parameters for controlling ultrafast magnetic field generation. One can also explore coherent electron dynamics by measurements of the temporal magnetic field dynamics. The present demonstration paves the way to induce and control intense magnetic fields by intense ultrafast circularly polarized laser pulses, which in principle, can be extended to other complex molecular systems and surfaces, and therefore has great potential for studying electron dynamics in ultrafast magneto-optics [40], the study of attosecond dynamics of nuclear processes at very high intensities [41], and molecular chiral properties [42].

ACKNOWLEDGMENTS

The authors thank Compute Canada for access to massively parallel computer clusters and NSERC, FQRNT for support of this research. J.G. also acknowledges support from National Natural Science Foundation of China under Grant No. 11574117.

[1] T. Brabec and F. Krausz, Rev. Mod. Phys. **72**, 545 (2000).
[2] F. Krausz and M. Ivanov, Rev. Mod. Phys. **81**, 163 (2009).
[3] K. Zhao, Q. Zhang, M. Chini, Y. Wu, X. Wang, and Z. Chang, Opt. Lett. **37**, 3891 (2012).
[4] N. Zhavoronkov and M. Ivanov, Opt. Lett. **42**, 4720 (2017).
[5] T. Gaumnitz, A. Jain, Y. Pertot, M. Huppert, I. Jordan, F. Ardana-Lamas, and H. J. Wörner, Opt. Express **25**, 27506 (2017).
[6] K. K. Lange, E. I. Tellgren, M. R. Hoffmann, and T. Helgaker, Science **337**, 327 (2012).
[7] A. Matos-Abiague and J. Berakdar, Phys. Rev. Lett. **94**, 166801 (2005).
[8] C. La-O-Vorakiat, E. Turgut, C. A. Teale, H. C. Kapteyn, M. M. Murnane, S. Mathias, M. Aeschlimann, C. M. Schneider, J. M. Shaw, H. T. Nembach, and T. J. Silva, Phys. Rev. X **2**, 011005 (2012).
[9] J.-Y. Bigot, M. Vomir, and E. Beaurepaire, Nat. Phys. **5**, 515 (2009).
[10] C. D. Stanciu, F. Hansteen, A. V. Kimel, A. Kirilyuk, A. T. Tsukamoto, A. Itoh, and T. Rasing, Phys. Rev. Lett. **99**, 047601 (2007).
[11] C.-H. Lambert1, S. Mangin, B. S. D. C. S. Varaprasad, Y. K. Takahashi, M. Hehn, M. Cinchetti, G. Malinowski, K. Hono, Y. Fainman, M. Aeschlimann, and E. E. Fullerton, Science **345**, 1337 (2014).
[12] B. Vodungbo, J. Gautier, G. Lambert, A. B. Sardinha, M. Lozano, S. Sebban, M. Ducousso, W. Boutu, K. Li, B. Tudu, M. Tortarolo, R. Hawaldar, R. Delaunay, V. López-Flores, J. Arabski, C. Boeglin, H. Merdji, P. Zeitoun, and J. Luning, Nat. Commun. **3**, 999 (2012).
[13] G. P. Zhang, W. Hübner, G. Lefkidis, Y. Bai, and T. F. George, Nat. Phys. **5**, 499 (2009).
[14] G. P. Zhan, Y. Bai, W. Hübner, G. Lefkidis, and T. F. George, J. Appl. Phys. **103**, 07B113 (2008).
[15] I. Barth, J. Manz, Y. Shigeta, and K. Yagi, J. Am. Chem. Soc. **128**, 7043 (2006).
[16] I. Barth and J. Manz, Phys. Rev. A **75**, 012510 (2007).
[17] K. Nobusada and K. Yabana, Phys. Rev. A **75**, 032518 (2007).
[18] M. Kanno, H. Kono, Y. Fujimura,, and S. H. Lin, Phys. Rev. Lett. **104**, 108302 (2010).
[19] E. Rasanen, A. Castro, J. Werschnik, A. Rubio, and E. K. U. Gross, Phys. Rev. Lett. **98**, 157404 (2007).
[20] K. J. Yuan and A. D. Bandrauk, Phys. Rev. A **88**, 013417 (2013).
[21] A. D. Bandrauk, J. Guo, and K.-J. Yuan, J. Opt. **19**, 124016 (2017).
[22] A. D. Bandrauk, S. Chelkowski, and H. S. Nguyen, Int. J. Quantum Chem. **100**, 834 (2004).
[23] H. C. Shao and A. F. Starace, Phys. Rev. Lett. **105**, 263201 (2010).
[24] F. Remacle and R. D. Levine, Proc. Natl. Acad. Sci. USA **103**, 6793 (2006).
[25] L. S. Cederbaum and J. Zobeley, Chem. Phys. Lett. **307**, 205 (1999).
[26] V. Despré, A. Marciniak, V. Loriot, M. C. E. Galbraith, A. Rouzeé, M. J. J. Vrakking, F. Lépine, and A. I. Kuleff, J. Phys. Chem. Lett. **6**, 426 (2015).
[27] A. I. Kuleff, N. V. Kryzhevoi, M. Pernpointner, and L. S. Cederbaum, Phys. Rev. Lett. **117**, 093002 (2016).
[28] G. Hermann, C. Liu, J. Manz, B. Paulus, J. F. Pérez-Torres, V. Pohl, and J. C. Tremblay, J. Phys. Chem. A **120**, 5360 (2016).

[29] D. Jia, J. Manz, B. Paulus, V. Pohl, J. C. Tremblay, and Y. Yang, Chem. Phys. **482**, 146 (2017).
[30] P. M. Kraus, B. Mignolet, D. Baykusheva, A. Rupenyan, L. Horný, E. F. Penka, G. Grassi, O. I. Tolstikhin, J. Schneider, F. Jensen, L. B. Madsen, A. D. Bandrauk, F. Remacle, and H. J. Wörner, Science **350**, 790 (2015).
[31] K. J. Yuan, C. C. Shu, D. Dong, and A. D. Bandrauk, J. Phys. Chem. Lett. **8**, 2229 (2017).
[32] K. J. Yuan and A. D. Bandrauk, Phys. Chem. Chem. Phys. **19**, 25846 (2017).
[33] K. J. Yuan, H. Z. Lu, and A. D. Bandrauk, Phys. Rev. A **83**, 043418 (2011).
[34] K. F. Lee, D. M. Villeneuve, P. B. Corkum, A. Stolow, and J. G. Underwood, Phys. Rev. Lett. **97**, 173001 (2006).
[35] A. D. Bandrauk and H. Shen, J. Chem. Phys. **99**, 1185 (1993).
[36] K. J. Yuan, H. Z. Lu, and A. D. Bandrauk, Phys. Rev. A **80**, 061403 (2009).
[37] O. D. Jefimenko, *Electricity and Magnetism: An Introduction to the Theory of Electric and Magnetic Fields* (Electret Scientific, Waynesburg, 1989).
[38] G. Lagmago Kamta and A. D. Bandrauk, Phys. Rev. A **75**, 041401(R) (2007).
[39] M. Kanno, H. Kono, S. H. Lin, and Y. Fujimura, in *Quantum Systems in Chemistry and Physics, Progress in Methods and Applications*, edited by K. Nishikawa, J. Maruani, E. J. Brändas, G. Delgado-Barrio, and P. Piecuch (Springer, Dordrecht, 2012).
[40] G. P. Zhang and T. F. George, Phys. Rev. B **78**, 052407 (2008).
[41] N. Milosevic, P. B. Corkum, and T. Brabec, Phys. Rev. Lett. **92**, 013002 (2004).
[42] O. Neufeld and O. Cohen, Phys. Rev. Lett. **120**, 133206 (2018).